Optical absorption spectra and magnetic susceptibilities of $PrVO_4$

K. Das, J. Jana, A. Sengupta, and D. Ghosh
Department of Solid State Physics, Indian Association for the Cultivation of Science, Jadavpur, Calcutta-700032

B. M. Wanklyn
Clarendon Laboratory, University of Oxford, Oxford, United Kingdom

(Received 13 March 1998; revised manuscript received 26 May 1998)

This paper reports experimental results of measurements of magnetic susceptibilities $\chi_{\parallel}$ and $\chi_{\perp}$ and their anisotropy $\Delta\chi$, in the temperature range of 300–70 K and the polarized optical-absorption and Zeeman spectra at temperatures 10 and 80 K of single crystal of $PrVO_4$. The magnetic anisotropy reversed its sign at 180 ± 2 K and two lines of the $^3H_4 \rightarrow {}^1D_2$ transitions split by 5.1 and 4.7 cm^{-1} in the Zeeman field of 49 K G. The lowest two levels were found to be singlets, separated by 35 ± 2 cm^{-1} and followed by a doublet at 84 ± 2 cm^{-1}. The observed magnetic results on $\chi_{\parallel}$, $\chi_{\perp}$, $\Delta\chi$, T_i and crystal-field (CF) levels of $^1D_2$, $^3P_{0,1,2}$, and $^1I_6$ multiplets and the Zeeman splittings were fitted simultaneously considering intermediate-coupling states mixed under a crystal field with D_{2d} symmetry present in $PrVO_4$. The best fitted parameters are $E^1 = 4425.0$, $E^2 = 22.7$, $E^3 = 455.0$, $\zeta = 800.0$, $\alpha = 22.5$, $\beta = -800.0$, $\gamma = 1520.0$, $B_{20} = -130$, $B_{40} = 1020$, $B_{44} = 1525$, $B_{60} = 1150$, $B_{64} = -200$ (all in cm^{-1}). Using the *J*-mixed pattern of $^3H_4$, the different components of the nuclear quadrupole splitting $4P$, were found to be $4P_1 = 3.2$, $4P_2 = 12.0$, and $4P_3 = 0.2$ (all in MHz) at 1.6 K. These results are close to the values reported from NMR studies by others. Schottky component of electronic and nuclear specific heat are also calculated with the best fitted CF levels of $^3H_4$. [S0163-1829(98)07437-2]

I. INTRODUCTION

The trivalent rare-earth (RE) ions in RE vanadates or in yttrium vanadate have received considerable attention since the last two decades as they find numerous applications in different fields and for their interesting magnetic, optical, and other thermophysical properties, exhibiting Jahn-Teller-induced crystallographic and magnetic phase transitions at low temperatures in some cases.[1–27]

Nd^{3+} and Ho^{3+} in YVO_4 have been found to be efficient laser materials.[12,5] $PrVO_4$ and $HoVO_4$ have been found to be suitable for enhanced nuclear magnetic cooling by isentropic demagnetization and can be used as an efficient refrigerant in the millikelvin region.[18] Eu^{3+}:YVO_4 in high-pressure mercury vapor lamps improves appearance and color.[2] Recently, extensive study on defect sites in $EuVO_4$, by spectral hole burning and optically detected nuclear quadrupole resonance techniques, using standard crystal-field (CF) analysis, have been reported.[14,20,21,24,27] These characteristics of RVO_4 and R:YVO_4 are strongly influenced by the environment of RE ions in the vanadate lattice, i.e., CF effect on the RE ion. Furthermore these substances are specially suitable for studies of CF interactions since their crystallographic structure is simple and the CF splitting of levels of the RE ions can be described by few parameters. The RVO_4 crystals have the tetragonal zircon structure at room temperature with space group D_{4h}^{19} $(I4_1/amd)$ and lattice parameters as given in Ref. 28. The O^{2-} ions forming a tetrahedra around the R^{3+} ion,[28,29] produce a CF at the R^{3+} ion site, which has D_{2d} $(42m)$ point-group symmetry, the tetragonal axis of which coincides with the crystalline *c* axis.

The present study on $PrVO_4$ involving measurements of the molecular magnetic susceptibilities $\chi_{\parallel}$, $\chi_{\perp}$, which are, respectively, parallel and perpendicular to the *c* axis, their anisotropy $\pm(\chi_{\parallel} - \chi_{\perp}) = \Delta\chi$ between 300 and 70 K as well as the polarized optical absorption and Zeeman spectra at 80 and 10 K were undertaken since there are few anomalies and uncertainties in the values of the CF parameters (CFP's) and level pattern of the lowest multiplet as reported from previous magnetic,[17] optical, and NMR (Refs. 10, 11) studies as discussed below.

From NMR spectral study of ^{141}Pr (and ^{51}V) in $PrVO_4$, Bleaney *et al.*[10] found that the lowest two CF levels are singlet levels, separated by about 100 cm^{-1}, however from later studies of the fluorescence, Raman, and far-infrared spectra[11] they observed the first excited singlet level to be at about 35 cm^{-1} followed by a doublet at 84 cm^{-1}. The remaining levels of $^3H_4$ manifold were estimated by an extrapolation procedure, which were therefore not accurately determined.

Bleaney *et al.*[11] also measured $\chi_{\perp}$ of a single crystal of $PrVO_4$ as well as the mean susceptibility $\bar{\chi} = (\chi_{\parallel} + 2\chi_{\perp})/3$ using the Faraday method. It was observed by them that although the calculated and observed values of $\chi_{\perp}$ were close (within 2%) around 4 K, as the temperature increased, the experimental values of $\chi_{\perp}$ fell off more steeply than the calculated results, becoming 10% less at 80 K. This discrepancy at the higher temperature region could not be attributed to the small changes in the energy values of the first and second excited CF levels of $^3H_4$ with temperature, which they observed from the fluorescence study, but was supposed to be due to the neglect of the excited multiplets in the theoretical expressions for the susceptibilities.[11] They also found that $PrVO_4$ retained tetragonal symmetry down to 1.6 K, unlike $TbVO_4$, $DyVO_4$, and $TmVO_4$ which undergo crystallographic or magnetic phase transition to a lower symme-

try at low temperatures, so the said discrepancy was not due to any such phase changes.

Guo, Aldred, and Chan[17] studied the thermal variation of $\overline{\chi}$ of $PrVO_4$ between 300 and 3.5 K and reported the values of CFP's and suggested the first excited level of $^3H_4$ to be at 90 cm^{-1}. Now, it is well known that CF analysis of $\overline{\chi}$ does not often give a unique set of CFP's, since $\overline{\chi}$ is an average property.[30] On the other hand, from fitting of the thermal characteristics of $\chi_\parallel$, $\chi_\perp$, $\Delta\chi$, and $\overline{\chi}$ with the corresponding theoretical expressions, deduced rigorously using *j* mixing of the relevant intermediately coupled (IC) states of Pr^{3+} under CF interaction, it is possible to determine very accurately the free ion (FI) and the CFP's as have been shown by us[31,32] and others.[33,34] Furthermore, the correct CF levels and states of $^3H_4$ were utilized to calculate other thermophysical properties associated with the ground term of $PrVO_4$, e.g., hyperfine interaction energies and paramagnetic Schottky specific heat for the electronic (C_{sh}) and nuclear (C_{shn}) level patterns, as was done by us earlier.[30–32,35–38]

II. THEORETICAL CONSIDERATIONS

The first step in our calculation was to diagonalize a free-ion Hamiltonian in a 13 Russell-Saunders (RS) basis of *LSJ* states consisting of Coulomb, spin-orbit, and configuration interactions to get the IC wave functions. The free-ion Hamiltonian H_{FI} used is as given below and described elsewhere:[31]

$$H_{\mathrm{FI}}=E^1e^1+E^2e^2+E^3e^3 + \zeta\sum_i 1_i\cdot s_i+\alpha L(L+1)+\beta G(G_2)+\gamma G(R_7).$$

For D_{2d} symmetry the CF perturbation H_{CF} has the form

$$H_{\mathrm{CF}}=B_{20}U_{20}+B_{40}U_{40}+B_{44}(U_{44}+U_{4-4}) + B_{60}U_{60}+B_{64}(U_{64}+U_{6-4}),$$

where the symbols are described elsewhere.[31]

Considering the total effective atomic Hamiltonian $H_{\mathrm{eff}}=H_{\mathrm{FI}}+H_{\mathrm{CF}}$, the combined FI and CF matrices were diagonalized in the 91 $|SLJM_J\rangle$ basis for the $4f^2$ ground configuration of Pr^{3+} to obtain all the CF levels and CF wave functions of $PrVO_4$ considering full *J* mixing under CF. The FI and CF parameters were varied to fit the optical and magnetic results simultaneously.[31] The FI parameters, chosen initially for determining IC wave functions, are those appropriate for triply ionized Pr^{3+} ions in $LaCl_3$.[39] However the final parameters were obtained by us from fitting our results. The same CF eigenvalues and wave functions are used to deduce expressions for the susceptibilities $\chi_\parallel$ and $\chi_\perp$ according to Van Vleck's formulas,[40] the splitting factor $g_\parallel$ ($g_\perp=0$) for each CF doublet levels, hyperfine energies, C_{sh} and C_{shn}.

III. EXPERIMENTAL RESULTS

$PrVO_4$ single crystals (dimensions~10 mm×1 mm ×1 mm) of very good quality were grown in the Clarendon Laboratory, from lead vanadate flux and recovered by hot pouring.[41] The thick rodlike crystals are transparent, light green in color and are elongated along the tetragonal *c* axis. Using a polarizing microscope single crystals were selected, followed by identification of the *c* axis and mounted as required for both the optical and magnetic measurements.

A. Polarized absorption spectral study

The polarized absorption spectra and Zeeman spectra of $PrVO_4$ were obtained in the range of 6200–4300 Å at 80 and 10 K using a Carl Zeiss Spectrograph (PGS-2), having high resolution with dispersions 3.38–3.55 Å/mm in the second order. The absolute accuracy is within 2 cm^{-1} for most of the lines and the relative accuracy for some is 1 cm^{-1} and the results obtained in this manner are reproducible to less than 0.5 Å over the entire range. The crystal was mounted on a copper sheet which was bolted to the cold tip of an optical shroud of a closed-cycle helium cryocooler (Displex CS 202). Spectra were taken for light propagating perpendicular to the *c* axis of the crystal, with polarization parallel (π) and perpendicular (σ) to the axis and also the axial spectra (light propagating along the *c* axis of the crystal) were taken to confirm the transitions to be electric dipole allowed. Zeeman spectra were recorded under a high pulsed magnetic field (49 K G) applied parallel to the *c* axis and was perpendicular to the propagation of light, details of which are given elsewhere.[42] A xenon lamp was used as a light source for the Zeeman study. Suitable filters were used to remove unwanted light and to avoid unnecessary heating of the crystal. The spectra in both the above cases were obtained on photographic films (ORWO NP77), which were then scanned by a sensitive solid-state microphotometric arrangement, connected to an *XY* recorder (Rikadenki RW 201). Spectral lines were calibrated by mercury lines. Figures 1–3 show the microphotometric traces of the different observed polarized absorption and Zeeman spectral lines of $^1D_2$, $^3P_0$, $^3P_1$, $^1I_6$, and $^3P_2$ multiplets of $PrVO_4$. Zeeman splitting was observed in the $^1D_2$ multiplet only.

B. Magnetic susceptibility

In $PrVO_4$ there are four magnetically equivalent molecules per unit cell, the D_{2d} axis of each being along the *c* axis. For such a reason, the axes of the molecular susceptibilities tensors $\chi_\parallel$ and $\chi_\perp$ are along the *c* and *a* axes, respectively,[43] consequently experimental work was very convenient and the results are very accurate. We measured the susceptibility $\chi_\perp$ in a Curie-type balance using the Faraday method[31,44] and the anisotropy $\Delta\chi$ using the static torque method[31,45] between 300 and 70 K. Experiments were done with three crystals of masses varying from 10 to 20 mg and the accuracy of the susceptibility results was within 1%.

While measuring $\Delta\chi$ at room temperature (RT), we observed that when the crystal was freely suspended vertically (*z*) with a very fine quartz fibre (drawn in the laboratory) with its *ac* plane placed horizontally (*xy*) inside a very homogeneous magnetic field ($H_x=3.5$ KG), then the *c* axis set was parallel to the applied field. This implied that $\chi_\parallel>\chi_\perp$ and the value of $\Delta\chi=\chi_\parallel-\chi_\perp$ was found to be 231 $\times10^{-6}$ emu/mole at 300 K which is only 4.6% of $\overline{\chi}$.[17] The corresponding values for PrES,[46] PrDG,[31] $Pr(OH)_3$,[37] and $PrCl_3$ (Ref. 47) are, respectively, 171, 353, 1493, and 740, all expressed in 10^{-6} emu/mole unit. On cooling below RT, $\Delta\chi$ decreased very slowly and approached zero at 180 ± 2 K (T_i)

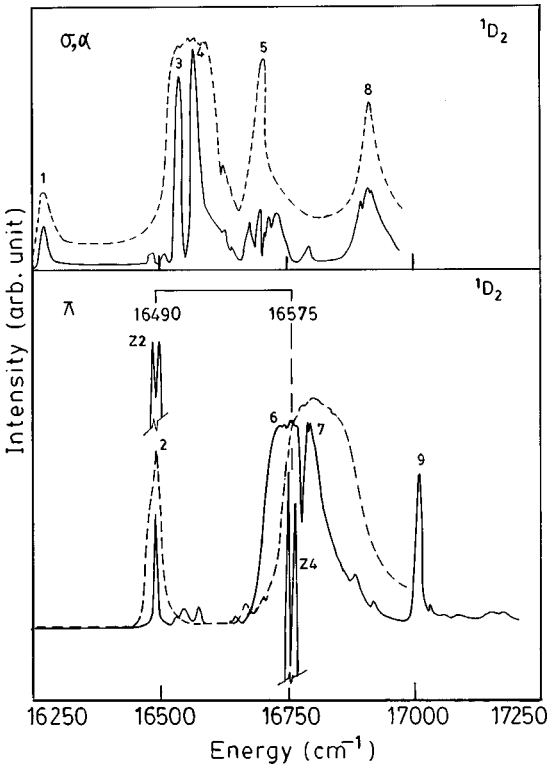

FIG. 1. Polarized absorption and Zeeman spectra for the transitions $^3H_4 \rightarrow {}^1D_2$ at 10 K (——) and 80 K (– – –). Absorption lines 1–9 correspond to transitions mentioned in text. $Z2$ and $Z4$ are Zeeman transitions corresponding to the absorption lines 2 and 4, respectively.

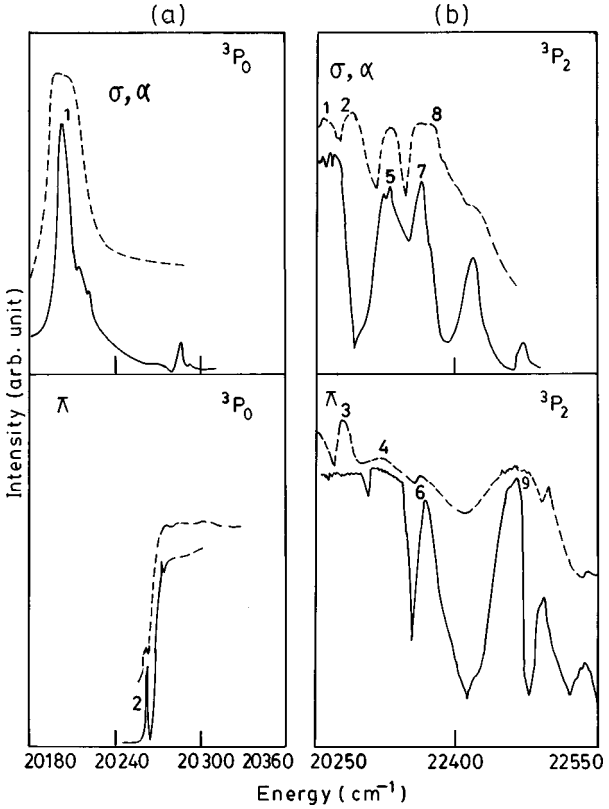

FIG. 2. Polarized absorption spectra at 10 K (——) and 80 K (– – –) for the transitions (a) $^3H_4 \rightarrow {}^3P_0$ and (b) $^3H_4 \rightarrow {}^3P_2$. See text for origin of absorption lines 1, 2 for (a) and 1 to 9.

and the crystal sharply rotated by 90° so that the a axis set along the applied field, indicating that $\chi_\perp$ became greater than $\chi_\parallel$. On further cooling, $\chi_\perp - \chi_\parallel$ increased more rapidly and was equal to 3440×10^{-6} emu/mole at 70 K (Fig. 4).

The thermal characteristics of $\chi_\parallel$ and $\chi_\perp$ showed the following Curie-Weiss behavior at higher temperatures due to the average contributions from all the CF levels of the $^3H_4$ term:

$$\chi_\parallel = \frac{1.84}{T + 71.78} \quad (300-100),$$

$$\chi_\perp = \frac{1.51}{T + 21.21} \quad (300-70).$$

The Curie constants along and perpendicular to the D_{2d} symmetry axis are modified from the free-ion value of 1.63 emu K. Magnetic moments $\mu_\parallel$ and $\mu_\perp$ are also found to exhibit CF effects but the average value μ_{eff} of these magnetic moments is $3.53\mu_\beta$, which is quite close to the free-ion value of $3.58\mu_\beta$.

It is relevant to mention here that generally for single crystals of Pr^{3+} compounds, it has been found that the $\Delta\chi$ exhibits inversion characteristics at a low temperature (T_i, say).[31,37,46,47] Now T_i, as well as the thermal characteristics of $\chi_\parallel$, $\chi_\perp$, and $\Delta\chi$, depend sensitively on the CF parameters, since not all sets of CF parameters and their wave functions would simulate such an inversion characteristic. Since the

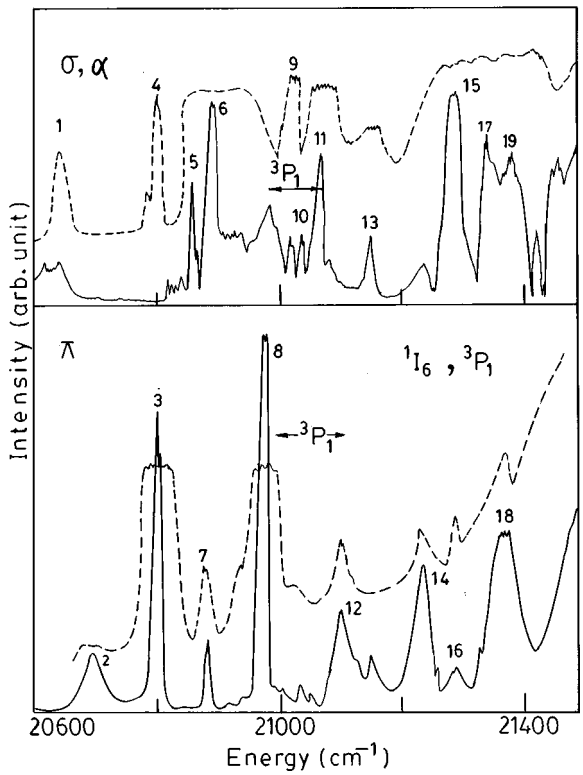

FIG. 3. Polarized absorption spectra for the transitions $^3H_4 \rightarrow {}^1I_6$ and $^3H_4 \rightarrow {}^3P_1$ at 10 K (——) and 80 K (– – –). Absorption lines 1–19 are the transitions mentioned in text.

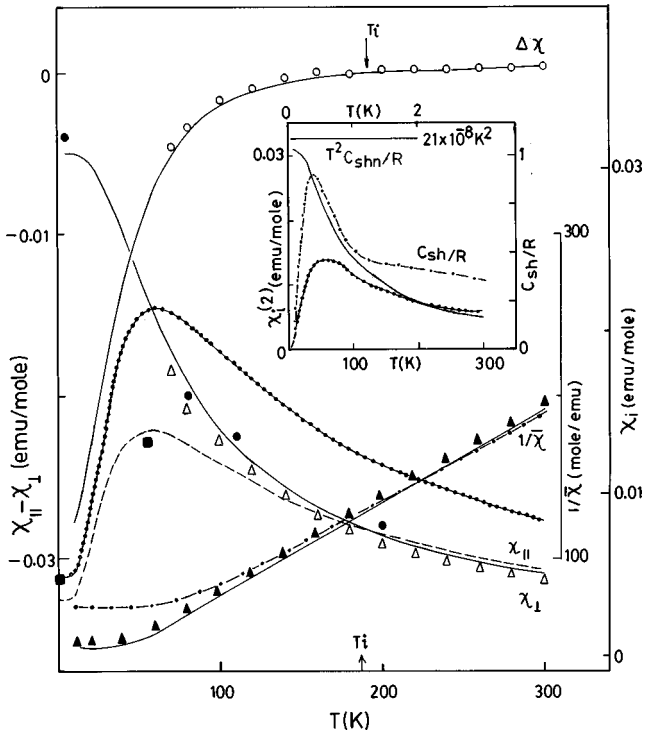

FIG. 4. Experimental thermal variations of $\Delta\chi$ (○), $\chi_\perp$ (△) from this work, $\chi_\perp$ (●) and $\chi_\parallel$ (■) are from Refs. 13 and 14, and $\overline{\chi}$ (▲) from Ref. 18. Solid and dashed lines correspond to our best fitted theoretical curves. $\chi_\parallel$ (· · · ·) and $\overline{\chi}$ (−·−·−·−) are theoretical curves corresponding to Refs. 11 and 17, respectively. Inset shows the second-order components of the theoretical curves of $\chi_\parallel^{(2)}$ (· · · ·) and $\chi_\perp^{(2)}$ (——) (see text). Schottky specific heat C_{sh}/R shows a maximum at 40 K and T^2C_{shn}/R is constant between 10 mk and 2 K (upper scale).

value of T_i can be determined very accurately using different crystals, T_i was considered as an important experimental parameter.

IV. DISCUSSIONS

A. Optical results

The assignments of crystal-field levels observed for the different multiplets were done considering D_{2d} site symmetry of Pr^{3+} in $PrVO_4$ and using the relevant selection rules.[1] Comparing the axial (α) spectra with the polarized spectra, it was found that for all the transitions the axial and σ-polarized spectra are identical and the π-polarized spectrum is unique, indicating the electric dipole nature of the transitions.

According to Bleaney *et al.*[11] the ground singlet is $|2^s\rangle$, i.e., B_1 and the first excited singlet $1A_1$ is $|4^s,0\rangle$, lying 35 cm^{-1} above it and the second excited state is a doublet $1E$ at 84 cm^{-1}. Our spectral amd magnetic results are also consistent with this pattern of $^3H_4$ (Tables I and II). Accordingly the observed CF levels were assigned as the following:

$$^3H_4(B_1,1A_1,1E);\quad ^1D_2(A_1,E,B_2,B_1)\quad ^3P_0(A_1);$$

$$^3P_1(E,A_2);\quad ^3P_2(A_1,B_2,E,B_1);$$

$$^1I_6(1B_2,1E,1A_1,A_2,2A_1,3E).$$

$^1D_2$

Figure 1 shows the 80 and 10 K absorption spectra for the transitions $^3H_4\rightarrow{}^1D_2$. At 10 K there is a very faint line (1) at 16 278 cm^{-1} in the σ polarization, which is more intensified at 80 K and is assigned as $1E(^3H_4)\rightarrow A_1(^1D_2)$. The two σ-polarized lines at 16 575 cm^{-1} (4) and 16 540 cm^{-1} (3) at 10 K and one π-polarized hot electronic line at 16 490 cm^{-1} (2) at 80 and 10 K are assigned as transitions $[B_1, 1A_1,$ and $1E(^3H_4)]\rightarrow E(^1D_2)$, respectively. The π-polarized line at 16 490 cm^{-1} ($Z2$) is split in the parallel Zeeman field at 10 K. The total splitting observed is 5.1 cm^{-1}, and the corresponding transitions are due to $\Delta M=0$ in π polarization, for a magnetic field parallel to the c axis of the crystal, where M is the magnetic quantum number of the Zeeman levels.[48] The observed Zeeman splitting of the transition $1E(^3H_4)\rightarrow E(^1D_2)$ arises due to the sum of splittings of the $1E(^3H_4)$ and $E(^1D_2)$. The faint π-polarized line at 16 575 cm^{-1} ($Z4$) splits by 4.7 cm^{-1} in the Zeeman spectra and gains in intensity, the cause of which may be that this transition is a magnetic-field induced magnetic dipole transition. Using these experimental results we found the splitting factors of $1E(^3H_4)$ and $E(^1D_2)$ to be 0.1735 and 2.0394, respectively, and the calculated values are close to these values (Table I).

The π-polarized lines at 16 790 cm^{-1} (7) and at 16 755 cm^{-1} (6), (the latter contained in the broadband) observed at 10 K and the σ-polarized hot line at 16 704 cm^{-1} (5) at 80 and 10 K were assigned, respectively, as transitions $[B_1, 1A_1,$ and $1E(^3H_4)]\rightarrow B_2(^1D_2)$. The π-polarized line at 17 006 cm^{-1} (9) at 10 K and σ-polarized line at 16 921 cm^{-1} (8) at 80 and 10 K are $[B_1$ and $1E(^3H_4)]$ $\rightarrow B_1(^1D_2)$.

$^3P_0$

Figure 2(a) shows the absorption spectra of transitions $^3H_4\rightarrow{}^3P_0$. The transitions $B_1(^3H_4)\rightarrow A_1(^3P_0)$ and $1A_1(^3H_4)\rightarrow A_1(^3P_0)$ are forbidden in π and σ polarizations. However a faint line at 20 262 cm^{-1} (2) was observed in π polarization at 10 K, which was identified as $1A_1(^3H_4)$ $\rightarrow A_1(^3P_0)$, from which the position of $A_1(^3P_0)$ came out to be 20 296 cm^{-1} matching the fluorescence spectral result.[11] It may be mentioned here that a very strong σ-polarized broadband around 20 200 cm^{-1} (1) was observed at 10 and 80 K which contained the transition $1E(^3H_4)\rightarrow A_1(^3P_0)$.

$^3P_2$

The spectral transitions from $^3H_4\rightarrow{}^3P_2$ are shown in Fig. 2(b). The σ-polarized line at 80 K at 22 254 cm^{-1} (1) was assigned as $1E(^3H_4)\rightarrow A_1(^3P_2)$. The transition $[B_1, 1A_1(^3H_4)]\rightarrow A_1(^3P_2)$ were not observed. The two π-polarized lines at 22 360 cm^{-1} (6), 22 326 cm^{-1} (4), and the σ-polarized line at 22 276 cm^{-1} (2) observed at 80 K were assigned as transitions $[B_1, 1A_1,$ and $1E(^3H_4)]\rightarrow B_2(^3P_2)$, respectively. The $1A_1(^3H_4)\rightarrow B_2(^3P_2)$ (4) transition is very broad. The transitions $[B_1, 1A_1,$ and $1E(^3H_4)]\rightarrow E(^3P_2)$ were identified with the σ-polarized lines at 22 366 cm^{-1} (7) and 22 332 cm^{-1} (5) and to the π-polarized line at 80 K at 22 282 cm^{-1} (3), respectively. The π-polarized weak line at

TABLE I. Energy eigenvalues (calculated and observed) of the multiplets of Pr^{3+} in $PrVO_4$. [The atomic parentages are the contributions (expressed in %) of different major multiplets, after J mixing by the crystal field. For all the multiplets, $g_{\|}$ values of doublets and D_{2d} states are given ($g_{\perp}$ being 0 for all the doublets). The values in the parenthesis are due to Bleaney *et al.* by an extrapolation method (Ref. 11)]. The parameters are $E^1=4425.0$, $E^2=22.7$, $E^3=455.0$, $\xi=800.0$, $\alpha=22.5$, $\beta=-800.0$, $\gamma=1520.0$, $B_{20}=-130$, $B_{40}=1020$, $B_{44}=1525$, $B_{60}=1150$, $B_{64}=-200$ (all in cm^{-1}).

Multiplets	D_{2d} states	Atomic parentage	Energy levels (in cm^{-1}) Observed	Calculated	$g_{\|}$
$^3H_4$	B_1	$96\%\,^3H_4+0.2\%\,^3F_2+3.5\%\,^1G_4$	0	0	
	$1A_1$	$95.9\%\,^3H_4+0.2\%\,^3F_4+3.6\%\,^1G_4$	35	35.7	
	$1E$	$95.4\%\,^3H_4+0.2\%\,^3F_4+3.6\%\,^1G_4+0.7\%\,^3H_5$	84	88.6	0.1096
	A_2	$95.8\%\,^3H_4+3.6\%\,^1G_4+0.4\%\,^3H_5+0.1\%\,^3F_3$	(127)	111	
	$2A_1$	$95.2\%\,^3H_4+3.6\%\,^1G_4+0.5\%\,^3H_5+0.4\%\,^3F_2$	(390)	288	
	B_2	$96.1\%\,^3H_4+3.6\%\,^1G_4+0.2\%\,^3H_5$	(276)	422	
	$2E$	$95.6\%\,^3H_4+0.2\%\,^3H_5+3.8\%\,^1G_4$	(600)	486	3.0873
$^1D_2$	B_2	$86.1\%\,^1D_2+10.4\%\,^3P_2+2.9\%\,^3F_2+0.6\%\,^1I_6$	16 362(A_1)	16 372	
	E	$87.2\%\,^1D_2+9.9\%\,^3P_2+2.8\%\,^3F_2$	16 575	16 562	2.0212
	A_1	$88.2\%\,^1D_2+9.1\%\,^3P_2+2.5\%\,^3F_2$	16 790(B_2)	16 808	
	B_1	$88.7\%\,^1D_2+8.5\%\,^3P_2+2.3\%\,^3F_2+0.5\%\,^1I_6$	17 006	17 022	
$^3P_0$	A_1	$97.8\%\,^3P_0+1.2\%\,^1S_0+0.8\%\,^1I_6$	20 296	20 313	
$^3P_1$	E	$99.9\%\,^3P_1$	21 064	21 011	2.9480
	A_2	$99.9\%\,^3P_1$	21 100	21 045	
$^1I_6$	$1A_1$	$98.6\%\,^1I_6+0.4\%\,^3H_6+0.7\%\,^3P_0$	20 730($1B_2$)	20 721	
	$1E$	$99.4\%\,^1I_6+0.4\%\,^3H_6$	20 880	20 744	2.8864
	$1B_2$	$99.1\%\,^1I_6+0.3\%\,^1D_2+0.4\%\,^3H_6$	20 884($1A_1$)	20 835	
	A_2	$99.5\%\,^1I_6+0.4\%\,^3H_6$		20 909	
	$2E$	$99.5\%\,^1I_6+0.4\%\,^3H_6$		20 917	3.1424
	$1B_1$	$99.5\%\,^1I_6+0.4\%\,^3H_6$		21 155	
	$2B_2$	$99.4\%\,^1I_6+0.2\%\,^1D_2+0.3\%\,^3H_6$	21 236(A_2)	21 208	
	$2A_1$	$99.4\%\,^1I_6+0.4\%\,^3H_6$	21 360	21 416	
	$3E$	$99.6\%\,^1I_6+0.4\%H_6$	21 370	21 424	0.0575
	$2B_1$	$99.1\%\,^1I_6+0.4\%\,^1D_2+0.4\%\,^3H_6$		21 468	
$^3P_2$	A_1	$90.7\%\,^3P_2+9.1\%\,^1D_2$	22 339	22 336	
	B_1	$91.3\%\,^3P_2+8.6\%\,^1D_2$	22 360(B_2)	22 358	
	E	$90.0\%\,^3P_2+9.7\%\,^1D_2+0.2\%\,^3F_2$	22 366	22 373	2.3697
	B_2	$89.4\%\,^3P_2+10.2\%\,^1D_2+0.3\%\,^3F_2$	22 458(B_1)	22 425	

22 458 cm^{-1} (9) and the σ-polarized line at 22 373 cm^{-1} (8) observed at 10 K were assigned as the transitions $[B_1,1E(^3H_4)]\rightarrow B_1(^3P_2)$.

$^3P_1$

Spectra of $^3H_4\rightarrow{}^3P_1$ at 80 and 10 K are shown in Fig. 3. There are two σ-polarized lines at 21 064 cm^{-1} (11) and 21 030 cm^{-1} (10) and one π-polarized hot electronic line at 20 977 cm^{-1} (8) at 80 and 10 K which are assigned as $[B_1, 1A_1,$ and $1E(^3H_4)]\rightarrow E(^3P_1)$ transitions, respectively. The π-polarized line at 21 100 cm^{-1} (12) and the σ-polarized hot line (increasing intensity at 80 K) at 21 014 cm^{-1} (9) were assigned as the electronic transitions B_1, $1E(^3H_4)\rightarrow A_2(^3P_1)$.

$^1I_6$

The transitions $^3H_4\rightarrow{}^1I_6$ are shown in Fig. 3. The π-polarized line at 20 696 cm^{-1} (2), appearing at 10 K, and the σ-polarized line at 20 635 cm^{-1} (1) at 80 K, are $1A_1$, $1E(^3H_4)\rightarrow B_2(^1I_6)$. Two σ-polarized lines at 20 880 cm^{-1} (6) and 20 845 cm^{-1} (5) at 10 K and the π-polarized line at 20 796 cm^{-1} (3) at 10 and 80 K are B_1, $1A_1$, and $1E(^3H_4)\rightarrow 1E(^1I_6)$. The π-polarized line at 20 884 cm^{-1} (7) at 10 and 80 K and σ-polarized line at 20 800 cm^{-1} (4) at 80 K (disappearing at 10 K) are assigned to B_1, $1E(^3H_4)\rightarrow 1A_1(^1I_6)$. The π-polarized line at 21 236 cm^{-1} (14) at 10 K and the σ-polarized line at 21 151 cm^{-1} (13) at 80 and 10 K are B_1, $1E(^3H_4)\rightarrow A_2(^1I_6)$. Similarly the π-polarized line at 21 360 cm^{-1} (18) and σ-polarized line at 21 278 cm^{-1} (15) at 10 K (the latter unresolved at 80 K) are assigned as B_1, $1E(^3H_4)\rightarrow 2A_1(^1I_6)$. The two σ-polarized lines at 21 370 cm^{-1} (19) and 21 337 cm^{-1} (17) at 10 K and the π-polarized line at 21 285 cm^{-1} (16) at 80 K are B_1, $1A_1$, and $1E(^3H_4)\rightarrow 3E(^1I_6)$. We could not assign the remaining levels of $^1I_6$ from the spectra since some lines in this region are not polarized and the 80 K spectra was not resolved as in the case of the other multiplets.

Often extra lines due to vibrational transitions have been observed in the different multiplets of rare-earth

TABLE II. Eigenvalues and eigenfunctions of the ground multiplet $^3H_4$ of $PrVO_4$.

Eigenvalues in cm^{-1}	Magnetic quantum No. (M)[a]	Eigenfunctions
0	2	$-0.693(\|^3H_4,+2\rangle+\|^3H_4,-2\rangle)-0.133(\|^1G_4,+2\rangle+\|^1G_4,-2\rangle)$
35.7	0	$0.603(\|^3H_4,+4\rangle+\|^3H_4,-4\rangle)+0.481\|^3H_4,0\rangle+0.117(\|^1G_4,+4\rangle+\|^1G_4,-4\rangle)+0.096\|^1G_4,0\rangle$
88.6	±1	$-0.844\|^3H_4,\pm1\rangle-0.491\|^3H_4,\mp3\rangle-0.164\|^1G_4,\pm1\rangle-0.097\|^1G_4,\mp3\rangle$
111.6	4	$0.692(\|^3H_4,+4\rangle-\|^3H_4,-4\rangle)+0.133(\|^1G_4,+4\rangle-\|^1G_4,-4\rangle)$
288	0	$0.338(\|^3H_4,+4\rangle+\|^3H_4,-4\rangle)-0.851\|^3H_4,0\rangle+0.065(\|^1G_4,+4\rangle+\|^1G_4,-4\rangle)-0.166\|^1G_4,0\rangle$
421.8	2	$-0.693(\|^3H_4,+2\rangle-\|^3H_4,-2\rangle)-0.135(\|^1G_4,+2\rangle-\|^1G_4,-2\rangle)$
486	±1	$0.493\|^3H_4,\pm1\rangle-0.844\|^3H_4,\mp3\rangle+0.098\|^1G_4,\pm1\rangle-0.167\|^1G_4,\mp3\rangle$

[a]Reference 48.

crystals[39,48–50] and vanadates.[11,21] It may be remarked that we observed also bands and some sharp lines between $^3P_0$ and $^1I_6$ and beyond $^1I_6$.

B. Magnetic susceptibilities results

Table II shows the J-mixed CF energy levels and wave functions of the ground term $^3H_4$. Due to want of space only those states which have sufficient admixtural coefficients with the 7 CF levels of the ground multiplet have been shown. It was found that CF mixings of $^3H_5$ with the lowest two CF levels of $^3H_4$ are only 0.15 and 0.05 % so that the effect of $^3H_5$ on the susceptibilities is negligible. Thus the discrepancy observed by Bleaney *et al.*[11] in the calculated and observed values of $\chi_\perp$ above 80 K cannot be attributed to their neglect of the effect of $^3H_5$.

The inversion characteristics of $\Delta\chi$ is a consequence of the different contributions of the directional susceptibilities $\chi_\parallel$ and $\chi_\perp$, in the first and second order, e.g., $\chi_\parallel^{(1)}$, $\chi_\perp^{(1)}$ and $\chi_\parallel^{(2)}$, $\chi_\perp^{(2)}$. Figure 4 (inset) shows the calculated thermal characteristics of these components. It was found that $\chi_\parallel^{(1)}$ is 135×10^{-6} emu/mole at RT which is only 2.6% of $\chi_\parallel$ and decreases by two orders at 10 K (not shown in Fig. 4). On the other hand, $\chi_\parallel^{(2)}$ shows a maximum at 56 K and is equal to 3200×10^{-6} emu/mole at 1 K. The lowest CF level is predominantly $-0.693(|+2\rangle+|-2\rangle)$ for which $\chi_\perp^{(1)}=0$. However there is appreciable contributions to $\chi_\perp^{(2)}$ from the excited levels through second-order interaction. At 300 K the contribution from the first doublet level is -6170×10^{-6} emu/mole which is comparable to that from the lower two singlets which are 7220×10^{-6} emu/mole and 4718×10^{-6} emu/mole, respectively. Thus on cooling, because of the depopulation effect of the third level, the value of $\chi_\perp$ increases quite sharply. These characteristics of $\chi_\parallel$ and $\chi_\perp$ thus explain the observed inversion of $\Delta\chi$.

It may be remarked here that Bleaney *et al.*[11] did not measure the thermal characteristics of $\chi_\parallel$, so we calculated the same (dotted line in Fig. 4), using their wave functions and energy-level pattern. It is obvious that the corresponding inversion of $\Delta\chi$ occurred at 53 K and the $\Delta\chi$ values are very different from our results. This is expected since, the magnetic anisotropy property is very sensitive to small changes on the CF wave functions. For this reason, it has been observed by us earlier[30–32,35–38] and others[34] that the latter can be very accurately determined when $\Delta\chi$ is studied accurately over a wide temperature region.

Again substituting the CF parameters of Guo, Aldred, and Chan[17] in our expression for the susceptibilities we found that the corresponding values of $\Delta\chi$ are widely different from our observed results, showing no inversion and that $\chi_\perp > \chi_\parallel$ between 300 and 4 K. This is obvious due to the fact that χ is an average property from which the CF parameters cannot be determined accurately.[30]

The above optical and magnetic results were thus explained very adequately by our CF levels and wave functions for which reason we used the same for calculating other physical properties of $PrVO_4$ which depend on $^3H_4$.

C. NMR results

Nuclear quadrupole splitting $4P$ of the ground nuclear state ($I_g=5/2$) occurs due to interaction between the nuclear quadrupole moment and the electric-field gradient at the ^{141}Pr nucleus, arising from the following three components:[10,11]

(1) The $4f$ contribution from the individual CF energy levels, weighted according to the Boltzmann function, is expressed as

$$P_1\left[I_z^2-\frac{1}{3}I(I+1)\right]$$

where

$$P_1=-[3e^2Q(1-R_Q)\langle r^{-3}\rangle_{4f}/4I(2I-1)]\times\langle J\|\alpha\|J\rangle\langle 3J_z^2-J(J+1)\rangle.$$

(2) The temperature-independent component due to asymmetry of lattice charges is defined as

$$P_3\left[I_z^2-\frac{1}{3}I(I+1)\right],$$

where

$$P_3=-\frac{3QA_2^0}{I(2I-1)\langle r^2\rangle_{4f}}\frac{(1-\gamma_\infty)}{(1-\sigma_2)}=-\frac{3Q}{I(2I-1)\langle r^2\rangle_{4f}}\frac{B_{20}}{2.7325202}\frac{(1-\gamma_\infty)}{(1-\sigma_2)}.$$

(3) A second-order contribution to the nuclear electric quadrupole interaction is written as

TABLE III. Observed (a) (Refs. 10 and 11) and calculated (b) resonance parameters and quadrupole splitting (expressed in MHz) of ^{141}Pr in $PrVO_4$. The constants used $Q=-0.0589$ b, $R_Q=0.1308$, $\langle r^{-3}\rangle_{4f}=5.369$ in atomic units (a.u.), $\langle J\|\alpha\|J\rangle=-0.021\,010\,1$, $\langle r^2\rangle_{4f}=1.086$ in a.u. and $(1-\gamma_\infty)/(1-\sigma_2)=206$.

Temperature (K)		20.4	15.3	4.2	1.6
$\gamma_\parallel/2\pi$	*a*	31.9	28.2	24.5	24.6
	b	31	26	20	20
$\gamma_\perp/2\pi$	*a*	76.6	77.4	77.7	77.6
	b	80	81	82	82
$4P_2/h$	*a*	7.1	9.5	10.3	10.3
	b	9	10	12	12
$4P_1/h$		2.5	2.9	3.2	3.2
$4P_3/h$		0.2	0.2	0.2	0.2
$4P/h$	*a*	11.1	12.3	13.4	13.5
	b	11.7	13.1	15.4	15.4

$$P_2\left[I_z^2-\frac{1}{3}I(I+1)\right] \quad \text{for } P_2=\frac{1}{2}(A_J/g_J\mu_B)\hbar\left(\frac{\gamma_\perp}{2\pi}-\frac{\gamma_{\rm II}}{2\pi}\right).$$

Values of different constants and experimental results[10,11] on $\gamma_\parallel$, $\gamma_\perp$, and $4P$ are given in Table III.

Each of the components of $4P$ (Table III) were calculated with the eigenvalues and eigenfunctions of $^3H_4$ (Table II), taking the *J*-mixed Lande splitting factor g_J of this IC state and substituting $A_J=1093$ MHz, corresponding to *LS* coupling which may often give an error as large as 4%.[51] Our calculated values of the thermal variations of $\gamma_\parallel/2\pi$ and $\gamma_\perp/2\pi$ are close to the observed values,[10,11] the small deviations can be removed by adjusting the A_J value slightly.

D. Specific heat

Generally, the rare-earth paramagnetic compounds have closely spaced low-lying CF levels for which reason the low-temperature specific heat C_p characteristics often show anomalous behavior due to paramagnetic Schottky specific-heat component $C_{\rm sh}$.[31,37,52] One (and sometimes 2) maximum is observed in the $C_{\rm sh}$ vs *T* curves and the value and the position of the maximum depend sensitively on the lowest CF levels. The expression for $C_{\rm sh}$ is given as

$$C_{\rm sh}=\frac{R}{Z^2}\left[Z\sum_{i=1}^{n}x_i^2\exp(-x_i)-\left\{\sum_{i=1}^{n}x_i\exp(-x_i)\right\}^2\right],$$

x being the *n* CF energy values divided by *kT*; *Z* and *R* are the partition function and gas constant, respectively. The thermal characteristic of $C_{\rm sh}$ was calculated using the same CF level pattern of $^3H_4$ obtained from best fitting of the optical and magnetic results, which has been shown in Fig. 4 (inset). Only one sharp peak at 40 K was expected. The Schottky specific heat $C_{\rm shn}$ corresponding to the nuclear levels was similarly calculated.[30] We found that $C_{\rm shn}$ has a peak at 0.2 mK and in the zero field, $T^2\ C_{\rm shn}/R=21\times10^{-8}$ K^2 remains constant between 10 mk and 2 K (Fig. 4 inset). Measurement of total specific heat C_p of $PrVO_4$ crystal in the low-temperature region is planned with the collaboration of Prof. E. Gmelin, Max Planck Institute.

It is relevant to mention that Bleaney[18] studied the changes in the entropy and nuclear specific heat of $PrVO_4$ with and without high magnetic field and noted that the linewidth $\Delta\nu$ observed was ten times the value obtained from the relation

$$T^2C_{\rm hf}/R=[2I(I+1)/9](h/k)^2(\Delta\nu^2)$$

for which anisotropic exchange or Jahn-Teller instability was proposed, since the Néel temperature was estimated to be around 0.006 mK.

V. CONCLUSION

Magnetic, optical, and the NMR results of $PrVO_4$ were reasonably well matched considering crystal-field mixing of the intermediately coupled states of the ground and excited states. However, there is further scope of closer fitting of the optical levels, especially for the $^1D_2$ multiplet using spin-correlated crystal-field theory which has been recently, extensively used.[33,53]

ACKNOWLEDGMENT

We are grateful to Professor R. K. Mukherjee for allowing us to use the spectrograph facilities.

[1] C. Brecher, H. Samelson, A. Lempicki, R. Riley, and T. Peters, Phys. Rev. **155**, 178 (1967).
[2] W. L. Wanmaker and J. W. Vrugt, Light. Res. Technol. **3**, 147 (1971).
[3] N. Karayianis, C. A. Morrison, and D. E. Wortman, J. Chem. Phys. **62**, 4125 (1975).
[4] G. A. Gehring and K. A. Gehring, Rep. Prog. Phys. **38**, 1 (1975).
[5] J. A. Wunderlich, J. G. Sliney, and L. G. Deshazer, IEEE J. Quantum Electron. **13**, 69 (1977).
[6] V. Kumar, J. Vishwamittar, and K. Chandra, J. Phys. C **10**, 267 (1977).
[7] A. Kasten and P. J. Becker, Phys. Status Solidi B **84**, 551 (1977).
[8] J. E. Battison, A. Kasten, M. J. M. Leask, and J. B. Lowry, J. Phys. C **10**, 323 (1977).
[9] B. Bleaney, A. H. Cooke, F. N. H. Robinson, and M. R. Wells, Physica B&C **86–88**, 1145 (1977).
[10] B. Bleaney, F. N. H. Robinson, S. H. Smith, and M. R. Wells, J. Phys. C **10**, L385 (1977).
[11] B. Bleaney, R. T. Harley, J. F. Ryan, M. R. Wells, and M. C. K. Wiltshire, J. Phys. C **11**, 3058 (1978).
[12] T. S. Lomheim and L. G. De Shazer, J. Appl. Phys. **49**, 5527 (1978).
[13] B. Bleaney, A. C. de Oliveira, and M. R. Wells, J. Phys. C **15**, 5275 (1982).

[14] R. L. Cone, R. T. Harley, and M. J. M. Leask, J. Phys. C **17**, 3101 (1984).
[15] Y. P. Yadava, R. A. Singh, and B. M. Wanklyn, J. Mater. Sci. Lett. **4**, 224 (1985).
[16] D. Neogy, A. K. Mukherjee, and A. Chatterjee, J. Phys. Chem. Solids **46**, 175 (1985).
[17] M. D. Guo, A. T. Aldred, and S. K. Chan, J. Phys. Chem. Solids **48**, 229 (1987).
[18] B. Bleaney, J. Phys.: Condens. Matter **2**, 7265 (1990).
[19] E. Antic-Fidancer, J. Holsa, M. Lemaitre-Blaise, and P. Porcher, J. Phys.: Condens. Matter **3**, 6829 (1991).
[20] R. L. Cone, P. C. Hansen, and M. J. M. Leask, J. Opt. Soc. Am. B **9**, 779 (1992).
[21] R. L. Cone, P. C. Hansen, M. J. M. Leask, and B. M. Wanklyn, J. Phys.: Condens. Matter **5**, 573 (1993).
[22] L. Zundu and H. Yidong, J. Phys.: Condens. Matter **6**, 3737 (1994).
[23] S. Skanthakumar, C. K. Loong, L. Soderholm, M. M. Abraham, and L. A. Boatner, Phys. Rev. B **51**, 12 451 (1995).
[24] B. Bleaney, Proc. R. Soc. London, Ser. A **450**, 711 (1995).
[25] P. K. Chakraborty, D. Neogy, K. N. Chattopadhayay, and B. M. Wanklyn, J. Phys. Chem. Solids **58**, 393 (1997).
[26] C. Xueyuan and L. Zundu, J. Phys.: Condens. Matter **9**, 7981 (1997).
[27] P. C. Hansen, M. J. M. Leask, B. M. Wanklyn, Y. Sun, R. L. Cone, and M. M. Abraham, Phys. Rev. B **56**, 7918 (1997).
[28] B. C. Chakoumakos, Marvin M. Abraham, and Lynn A. Boatner, J. Solid State Chem. **109**, 197 (1994).
[29] R. W. G. Wyckoff, *Crystal Structures 3* (Interscience, New York, 1965).
[30] S. Karmakar, M. Saha, and D. Ghosh, Phys. Rev. B **26**, 7023 (1982).
[31] K. Das and D. Ghosh, J. Phys. Chem. Solids **59**, 679 (1998).
[32] S. Jana, D. Ghosh, and B. M. Wanklyn, J. Magn. Magn. Mater. **183**, 135 (1998).
[33] G. W. Burdick, C. K. Jayasankar, F. S. Richardson, and M. F. Reid, Phys. Rev. B **50**, 16 309 (1994).
[34] D. Neogy, K. N. Chattopadhyay, P. K. Chakrabarty, H. Sen, and B. M. Wanklyn, J. Magn. Magn. Mater. **154**, 127 (1996).
[35] M. Saha and D. Ghosh, Phys. Rev. B **22**, 308 (1980).
[36] S. Dasgupta, M. Saha, S. Mroczkowski, and D. Ghosh, Phys. Rev. B **27**, 6960 (1983).
[37] T. Kundu, D. Ghosh, and S. Mroczkowski, J. Phys. C **21**, 5993 (1988).
[38] A. Sengupta, D. Ghosh, and B. M. Wanklyn, Phys. Rev. B **47**, 8281 (1993).
[39] S. Hüfner, *Optical Spectra of Transparent Rare Earth Compounds* (Academic, New York, 1978).
[40] J. H. Van Vleck, *The Theory of Electronic and Magnetic Susceptibilities* (Oxford University Press, London, 1932).
[41] S. H. Smith and B. M. Wanklyn, J. Cryst. Growth **21**, 23 (1974).
[42] M. Chowdhury, R. K. Mukherjee, and S. C. Bera, Chem. Phys. **3**, 482 (1974).
[43] K. Longsdale, K. S. Krishnan, Proc. R. Soc. London, Ser. A **156**, 597 (1936).
[44] S. Chowdhuri, D. Ghosh, and A. K. Pal, Thin Solid Films **61**, 51 (1979).
[45] D. Guha Thakurta and D. Mukhopadhyay, Indian J. Phys. **40**, 69 (1966).
[46] K. H. Hellwege, W. Schembs, and B. Schneider, Z. Phys. **167**, 477 (1962).
[47] B. Schneider, Z. Phys. **177**, 179 (1964).
[48] G. H. Dieke, *Spectra and Energy Levels of Rare Earth Ions in Crystals* (Interscience, New York, 1968).
[49] B. R. Judd, *Handbook on the Physics and Chemistry of Rare Earths* (Elsevier Science, Amsterdam, 1988).
[50] H. P. Jenseen, A. Linz, R. P. Leavitt, C. A. Morrison, and D. E. Wortman, Phys. Rev. B **11**, 92 (1975).
[51] A. Abragam and B. Bleaney, *Electron Paramagnetic Resonance of Transition Ions* (Clarendon, Oxford, 1970), Chap. 5.
[52] R. D. Chirico, E. F. Westrum Jr., J. B. Gruber, and J. Warmkessel, J. Chem. Thermodyn. **11**, 835 (1979).
[53] A. Renuka Devi, C. K. Jayasankar, and M. F. Reid, Phys. Rev. B **49**, 12 551 (1994).